Transitional Shock-Wave / Boundary Layer Interaction behind a Roughness Element

Nicola De Tullio and Neil D. Sandham

1 Introduction

Interactions of shock-waves with boundary layers are a common feature in high-speed flight. Depending on the nature of the incoming boundary layer such interactions may lead to large unsteady thermal and pressure loads which may reduce the aerodynamic performance and the structural integrity of hypersonic vehicles. Despite numerous investigations our current knowledge of the fundamental physical mechanisms involved in unsteady shock-wave/boundary-layer interactions (SBLI) is far from complete and a number of aerospace applications would benefit from a deeper understanding of the subject. Most of the research efforts in this field have been directed to the analysis of shock-waves interacting with nominally two-dimensional turbulent boundary layers [1]. Flows over high-speed vehicles and, in particular, inside the intakes of their air-breathing propulsion systems are very complex and include interactions of shock-waves with three-dimensional transitional boundary layers. The transition process is very sensitive to flow conditions and geometric parameters. Experiments have shown that small roughness elements, less than a millimetre in height, can lead to early breakdown to turbulence even in a quiet environment [2]. In high-speed flows, transitional boundary layers can also be affected by the interaction with shock-waves through mechanisms which are largely unknown. A detailed study of three-dimensional transitional SBLI will help understand how shock-waves affect the transition process at high-speeds. The limited number of studies available in the literature on transitional SBLI show that for strong interactions (in the convective instability regime) small-amplitude disturbances experience strong amplification across the separation bubble due to the instability of the separated shear layer [3]. In addition, transitional interactions induce higher levels of unsteadiness and stronger thermal loads than in the fully turbulent case [4, 5].

Nicola De Tullio · Neil D. Sandham
School of Engineering Sciences, University of Southampton, Southampton SO17 1BJ, UK

The present work focuses on the interaction of a weak oblique shock-wave with the transitional boundary layer developing behind an isolated sharp-edged roughness element, complementing the previous work of [6]. The investigation is conducted by performing direct numerical simulations (DNS) of the transition process with and without SBLI, so that the effects of the shock interaction can be clearly seen by comparing the two resulting flow fields.

2 Methodology

The present study focuses on DNS of the compressible Navier-Stokes equations. The calculations were carried out using a parallel, multi-block code which uses a fourth-order central spatial differencing scheme. Time integration is based on a third-order compact Runge-Kutta method. An entropy splitting approach by Sandham *et al.* [7] is used to split the inviscid flux derivatives into conservative and non-conservative parts, thereby improving the stability of the non-dissipative central scheme. Periodic boundary conditions are applied in the spanwise direction, while the walls are considered no-slip and isothermal, with a temperature equal to the laminar adiabatic wall temperature. The reflection of waves from the domain external boundaries is minimised by using integrated characteristic conditions for the top and outflow boundaries. The inflow is initialised with the compressible laminar similarity solution and a pressure extrapolation boundary condition is then applied, whereby in the subsonic region of the boundary layer the inflow conservative variables are calculated by extrapolating the pressure from the domain using a first order approximation.The code was made parallel using the *MPI* library.

The impinging shock-wave was captured using the method of Yee *et al.* [8] coupled with the Ducros sensor [9]. The presence of a sharp-edged roughness element induces small spatial grid-to-grid-point oscillations in the density field due to an inherent discontinuity in the derivatives at the roughness edges. The computational grid was substantially refined near the roughness element and the residual spurious oscillations were treated using a sixth order filter by Visbal and Gaitonde [10]. The filter is applied at each time step and the conservative variables array ($\mathbf{U} = \{\rho, \rho u, \rho v, \rho w, \rho E\}^T$) is updated as follows

$$\mathbf{U} = \mathbf{U} - \sigma \left(\mathbf{U} - \mathbf{U}_{filtered} \right), \tag{1}$$

where $\sigma = 0.05$ so that only 5% of the filtered field was used.

The transition process is initiated by forcing a small broadband acoustic disturbance in the free-stream upstream of the roughness element. The forcing takes the following form

$$\rho(\mathbf{x}, t) = A \exp\left(-\tilde{r}^2\right) \sum_{m=1}^{M} \sum_{n=1}^{N} \cos\left(\beta_m z + \phi_m\right) \sin\left(\omega_n t + \phi_n\right), \tag{2}$$

where M and N are the total number of spanwise wavenumbers and frequencies respectively. The coordinate $\tilde{r}$ is defined as $\tilde{r}^2 = \left[(x-x_f)^2 + (y-y_f)^2\right]/L_f$, where L_f determines the radius of the forcing region and x_f and y_f its centre. Random phases ϕ are introduced to avoid spurious high amplitude peaks in the forcing signal which might trigger nonlinearities. The signal contains $N = 18$ non-dimensional frequencies in the range $0.06 - 0.4$ with steps of 0.02. Here the non-dimensional frequencies are expressed using the Strouhal number, defined in terms of the roughness height h^* and the reference velocity U^*_∞ as $St = f^* h^*/U^*_\infty$, where f^* is the dimensional frequency. The forcing contains $M = 25$ spanwise modulations. The amplitude $A = 6 \times 10^{-5}$ was selected to introduce disturbances in the linear regime. Note that here asterisks denote dimensional quantities.

3 Results

As already mentioned the present study focuses on the analysis of DNS data from two numerical simulations of transition induced by roughness with and without SBLI at Mach 2.5 and $Re_{\delta^*_{in}} = 3300$. The flow configuration and computational grid are shown in Table 1 and are the same for the two simulations analysed. The same table also reports the grid resolution in the turbulent boundary layer and information about the sample used to compute statistical data in the two cases. As can be noticed the interaction studied is relatively weak but still strong enough to trigger separation. Stronger interactions would induce big separation bubbles making the simulations both prohibitively expensive and difficult to compare with the case of no interaction. The grid spacings expressed in wall units are taken inside the turbulent wedge at $x/\delta^*_{in} \approx 240$. The spanwise grid spacing is expressed as an interval and increases from the roughness centerline to the sides of the turbulent wedge (due to the grid stretching applied). The grid resolution is typical of fully resolved DNS studies [11] for both cases, although the grid requirements increase in the shock interaction case.

Figure 1 shows instantaneous contours of the temperature field on the roughness centerline plane for the two cases analysed. The main features of the transition process can be inferred. The roughness induces a pair of counter-rotating streamwise vortices (not shown) which lift up low velocity fluid from the wall at the centerline, thereby creating a region of high shear detached from the wall. The small acoustic

Table 1 Simulation parameters, grid resolution and sampling information.

Wedge angle, degrees	0.0	1.93
$L_x \times L_y \times L_z/\delta^*_{in}$	$250\times20\times60$	$250\times20\times60$
$N_x \times N_y \times N_z$	$1989\times222\times547$	$1989\times222\times547$
Grid resolution, Δx^+, Δy^+_{min}, Δz^+	6.3, 0.73, [2.6, 7.6]	7.5, 0.9, [3.1, 9.3]
Observation period, $T_s U_\infty/\delta^*_{in}$	1200	1600
Sampling frequency, $f_s \delta^*_{in}/U_\infty$	0.1	0.1
Time step, $\Delta t U_\infty/\delta^*_{in}$	0.02	0.02

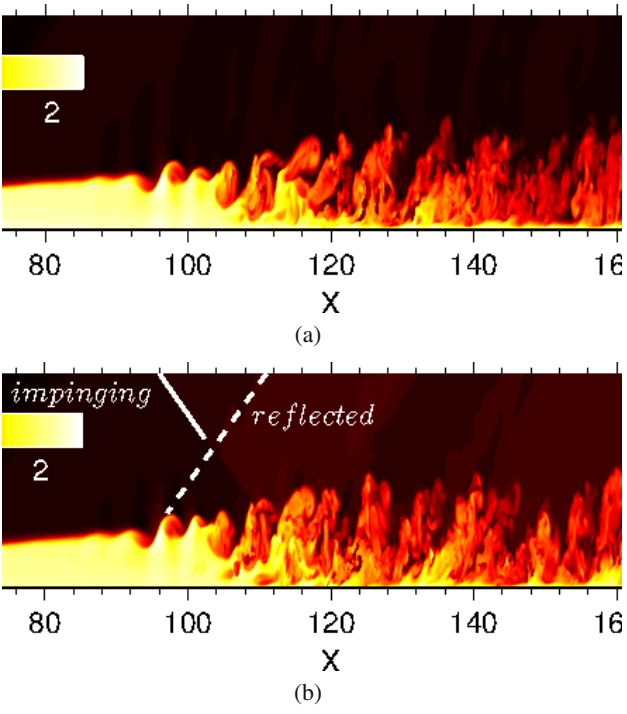

Fig. 1 Instantaneous contours of the temperature field. The white lines show the shock system and the balck lines indicate regions of separated flow.

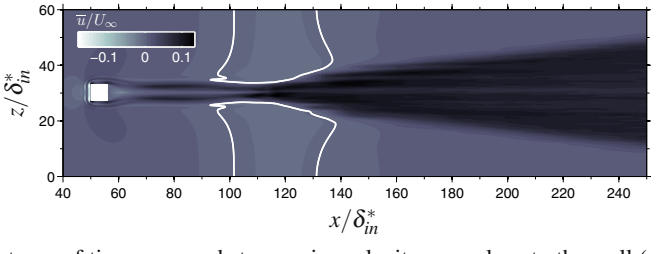

Fig. 2 Contours of time averaged streamwise velocity very close to the wall ($y/\delta^*_{in} = 0.03$). The white line shows the time-averaged separation bubble.

disturbances enter the shear layer and grow exponentially (initially) leading to the breakdown of the shear layer, which then quickly drives the transition of the entire boundary layer. The oblique shock is set to impinge at $x_{imp}/\delta^*_{in} = 118$ in a region of three-dimensional transitional flow. The initial growth of disturbances in the shear

layer is not affected by the interaction. The shock system, highlighted by the two white lines in the figure, is weak and does not separate the transitional/turbulent region of the boundary layer. On the other hand, a relatively large separation bubble is formed in the laminar region, as can be seen in figure 2, which shows time-averaged streamwise velocity contours near the wall. The white contour line shows the time-averaged separation bubble. The length L_{sep} of the bubble ranges from about 30 inflow displacement thicknesses at the sides of the domain to about 40 close to the transitional region. The figure also shows the foot-prints of a pair of co-rotating horseshoe vortices immediately upstream of the roughness element and the big streamwise vortices downstream of it. The latter seem to influence the boundary layer up to the end of the computational domain.

Figure 3 gives the skin friction at two different locations along the span, namely $z/\delta^*_{in} = 30$ (centerline) and $z/\delta^*_{in} = 36$. At the centerline the skin friction suddenly rises and overshoots the turbulent value, as expected for a transitional boundary layer. The shock displaces the skin friction peak slightly upstream and, more notably, increases the skin friction in the turbulent region downstream. At $z/\delta^*_{in} = 36$ transition happens significantly earlier in the case with shock impingement, suggesting an important effect of the interaction on the lateral spreading of turbulence. Comparing the skin friction at the two spanwise positions one can notice that the modifications induced by the roughness in the turbulent region of the boundary layer are not negligible.

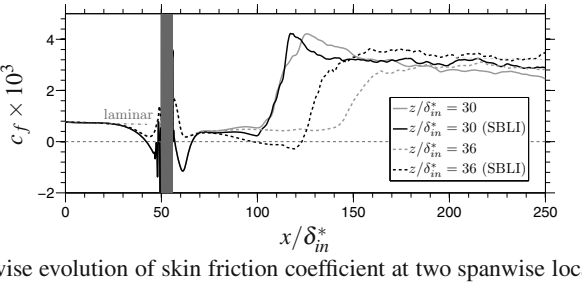

Fig. 3 Streamwise evolution of skin friction coefficient at two spanwise locations. The grey shaded area indicates the position of the roughness.

The lateral spreading of the turbulent wedge developing behind the roughness element is compared in figure 4, where the distribution of turbulent kinetic energy at $y = 1.0$ is plotted for the two cases. The effect of the impinging shock is to induce a region of high turbulent energy. In particular, the streamwise normal stress (not shown) accounts for the most energy. The region of amplified turbulent intensity is located at the sides of the turbulent wedge right after the shear-layer breakdown. Turbulence spreading is fast in these regions so that the wedge thickens rapidly. Further downstream the turbulence seems to recover the same spreading rate of the case without interaction.

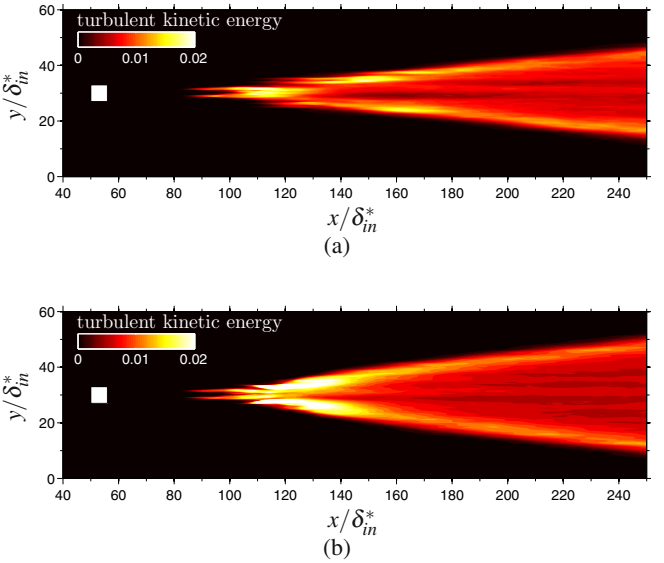

Fig. 4 Contours of turbulent kinetic energy at $y/\delta^*_{in} = 1.0$

4 Conclusion

The modifications induced by transitional SBLI in the roughness-induced transition process were studied by direct numerical simulations. Despite the relatively weak transitional interaction considered, the results show a big influence of the shock on the transition process and on the state of the turbulent boundary layer downstream of the interaction. The shock was found to enhance the lateral spreading of turbulence locally leading to a thicker turbulent wedge.

Acknowledgements. The work was performed within the Long-Term Advanced Propulsion Concepts and Technologies project investigating high-speed air breathing propulsion. LAPCAT II, coordinated by ESA-ESTEC, is supported by the EU within the 7th Framework Programme, Collaborative Project: Small or Medium- Scale Focused Research Project, Theme 7: TRANSPORT, contract no.: ACP7-GA-2008-211485. Further information on LAPCAT II can be found on `http://www.esa.int/techresources/lapcat`.

References

1. Dolling, D.S.: Fifty Years of Shock-Wave/Boundary-Layer Interaction Research: What Next? AIAA J 39(8), 1517–1531 (2001)
2. Schneider, S.P.: Effects of Roughness on Hypersonic Boundary-Layer Transition. J. Spacecraft and Rockets 45(2), 193–209 (2008)

3. Yao, Y., Krishnan, L., Sandham, N.D., Roberts, G.T.: The Effect of Mach Number on Unstable Disturbances in Shock/Boundary-Layer Interactions. Phys. Fluids 19, 054104 (2007)
4. Benay, R., Chanetz, B., Mangin, B., Vandomme, L., Perraud, J.: Shock Wave/Transitional Boundary-Layer Interactions in Hypersonic Flow. AIAA J. 44(6), 1243–1254 (2006)
5. Murphree, Z.R., Jagodzinski, J., Hood, E.S., Clemens, N.T., Dolling, D.S.: Experimental Studies of Transitional Boundary Layer Shock Wave Interactions. AIAA paper 2006-326 (2006)
6. Redford, A.J., Sandham, N.D., Roberts, G.T.: Compressibility Effects on Boundary-Layer Transition Induced by an Isolated Roughness Element. AIAA J. 48(12), 2818–2830 (2010)
7. Sandham, N.D., Li, Q., Yee, H.: Entropy Splitting for High-Order Numerical Simulation of Compressible Turbulence. J. Comput. Phys. 178, 307–322 (2002)
8. Yee, H.C., Sandham, N.D., Djomehri, M.J.: Low-Dissipative High-Order Shock-Capturing Methods using Characteristic-Based Filters. J. Comput. Phys. 150, 199–238 (1999)
9. Ducros, F., Ferrand, V., Nicoud, F., Weber, C., Darrac, D., Gacherieu, C., Poinsot, T.: Large-Eddy Simulation of the Shock/Turbulence Interaction. J. Comput. Phys. 152, 517–549 (1999)
10. Visbal, M.R., Gaitonde, D.V.: On the Use of High-Order Finite Difference Schemes on Curvilinear and Deforming Meshes. J. Comput. Phys. 181, 155–185 (2002)
11. Pirozzoli, S., Grasso, F., Gatski, T.B.: Direct Numerical Simulation and Analysis of a Spatially Evolving Supersonic Turbulent Boundary Layer at $M = 2.25$. Phys. Fluids 16(3), 530–545 (2004)